Biogeosciences Discuss., 12, 11661–11705, 2015
www.biogeosciences-discuss.net/12/11661/2015/
doi:10.5194/bgd-12-11661-2015

Biogeosciences Discussions
Open Access

Modern to millennium-old greenhouse gases emitted from freshwater ecosystems of the eastern Canadian Arctic

F. Bouchard[1,2,3], I. Laurion[1,3], V. Prėskienis[1,3], D. Fortier[2,3], X. Xu[4], and M. J. Whiticar[5]

[1]Centre Eau Terre Environnement, Institut national de la recherche scientifique, Québec, QC, G1K 9A9, Canada
[2]Département de géographie, Université de Montréal, Montréal, QC, H3C 3J7, Canada
[3]Centre d'études nordiques, Université Laval, Québec, QC, G1V 0A6, Canada
[4]Department of Earth System Science, University of California Irvine, Irvine, CA, 92697, USA
[5]Biogeochemistry Facility, School of Earth and Ocean Sciences, University of Victoria, Victoria, BC, V8W 3P6, Canada

Received: 1 July 2015 – Accepted: 10 July 2015 – Published: 24 July 2015

Correspondence to: F. Bouchard (frederic.bouchard@cen.ulaval.ca) and I. Laurion (isabelle.laurion@ete.inrs.ca)

Published by Copernicus Publications on behalf of the European Geosciences Union.

Abstract

Ponds and lakes are widespread across the rapidly changing permafrost environments. Aquatic systems play an important role in global biogeochemical cycles, especially in greenhouse gas (GHG) exchanges between terrestrial systems and the atmosphere. The source, speciation and emission of carbon released from permafrost landscapes are strongly influenced by local specific conditions rather than general environmental setting. This study reports on GHG ages and emission rates from aquatic systems on Bylot Island in the eastern Canadian Arctic. Dissolved and ebullition gas samples were collected during the summer season from different types of water bodies located in a highly dynamic periglacial valley: polygonal ponds, collapsed ice-wedge trough ponds, and larger lakes overlying unfrozen soils (talik). The results showed strikingly different ages and fluxes depending on aquatic system types. Polygonal ponds were net sinks of dissolved CO_2, but variable sources of dissolved CH_4. They presented the highest ebullition fluxes, one or two orders of magnitude higher than from other ponds and lakes. Trough ponds appeared as substantial GHG sources, especially when their edges were actively eroding. Both types of ponds produced modern to hundreds of years old (< 550 yr BP) GHG, even if trough ponds could contain much older carbon (> 2000 yr BP) derived from freshly eroded peat. Lakes had small dissolved and ebullition fluxes, however they released much older GHG, including millennium-old CH_4 (up to 3500 yr BP) sampled from lake central areas. Acetoclastic methanogenesis dominated at all study sites and there was minimal, if any, methane oxidation in gas emitted through ebullition. These findings provide new insights on the variable role of permafrost aquatic systems as a positive feedback mechanism on climate.

BGD
12, 11661–11705, 2015

1 Introduction

Climate warming impacts Arctic landscapes through permafrost thawing and erosion (Romanovsky et al., 2010). This results in the release of both old and recent organic carbon to the atmosphere as greenhouse gases (GHG) (Zimov et al., 2006; Schuur et al., 2015). Permafrost stores large quantities of carbon compared to the atmosphere, although quantitative estimates are still under discussion (Tarnocai et al., 2009; Hugelius et al., 2014). Widespread across permafrost environments, aquatic systems act as biogeochemical hotspots by releasing substantial amounts of carbon dioxide (CO_2) and methane (CH_4) (e.g., Walter et al., 2007; Laurion et al., 2010; Abnizova et al., 2012). It is generally considered that CH_4 ebullition is the main mechanism of GHG emissions from northern ponds and lakes, a transport mechanism highly heterogeneous in space and time (Wik et al., 2011). However, emissions through diffusion could be underestimated especially in the case of small systems, as flux values are often computed from wind-based empirical models developed for larger lakes located in different climatic regions (Bastviken et al., 2008; Tedford et al., 2014). Other processes involved in GHG dynamics, such as plant-mediated transport and microbial oxidation, also need to be considered in the specific context of the Arctic (Bastviken et al., 2004; Liebner et al., 2011). Moreover, lateral inputs of CH_4 produced within the active layer or lateral export of permafrost carbon away from thaw sites via streams and rivers were recently demonstrated (Vonk and Gustafsson, 2013; Godin et al., 2014; Paytan et al., 2015). Overall, thermokarst (thaw) ponds and lakes represent a major landscape feature in permafrost-affected regions (Grosse et al., 2013), and there is a growing interest in defining the specific role of various types of freshwater ecosystems in global carbon dynamics associated to permafrost degradation processes, and how they may rapidly respond to environmental changes.

Upscaling and modeling GHG emissions is challenging and oversimplified assumptions can lead to large calculations errors (Stepanenko et al., 2011; van Huissteden et al., 2011; Gao et al., 2013). The gaps that need to be fullfilled to model future

BGD
12, 11661–11705, 2015

GHG emissions with more accuracy include defining the vertical distribution of carbon in permafrost soils, the interactions between permafrost thaw and surface hydrology, as well as distinguishing CH_4 from CO_2 emissions and gradual warming from abrupt thaw mechanisms (Schuur et al., 2015). One important yet rarely considered aspect of aquatic system biogeochemistry is the age of carbon processed and released by these biogeosystems, which will determine the strength of their climate feedback effect. High GHG emissions (especially CH_4) from old (late Pleistocene-age) organic ice-rich loess permafrost (*yedoma*) have been reported from thermokarst lakes of Siberia and Alaska in regions that were not ice-covered during the last glaciation (Zimov et al., 1997; Brosius et al., 2012). In Canada, which accounts for a very large portion of circum-Arctic permafrost, these deposits are rare as the territory was almost entirely covered by ice during that period (Dyke and Prest, 1987). The carbon trapped in permafrost is thus younger (Holocene-age) in this part of the Northern Hemisphere (e.g., Allard, 1996; Burn and Kokelj, 2009; Lauriol et al., 2010; Tremblay et al., 2014). It nevertheless represents an excess carbon stock that can contribute as a positive climate feedback, compared to modern carbon that is used and recycled through short-term biogeochemical processes (photosynthetic fixation and microbial respiration). Preliminary data on GHG radiocarbon age from small tundra ponds of the eastern Canadian Arctic showed that the carbon released by these ecosystems was generally modern with a minor fraction of century-old gas at a few sites (Negandhi et al., 2013), thus mostly part of the natural carbon cycle which does not create positive climate feedback.

The objective of the present study was to characterize GHG composition, production pathway, age and emission rates in ponds and lakes on Bylot Island (Nunavut) in the eastern Canadian Arctic. We analyzed dissolved and ebullition gas samples collected in July from ponds and lakes located within an organic-rich permafrost terrace of Late Holocene age (Fortier et al., 2006).

BGD
12, 11661–11705, 2015

2 Study area

Bylot Island (Nunavut) is located in the eastern Canadian Arctic, within the continuous permafrost zone (Fig. 1). The sampling site is surrounded by the Byam Martin Mountains, which belong to the Davis Highlands physiographic region and run southeast–northwest across the island. The plains that stretch out on either side of the mountains belong to the Arctic Lowlands physiographic region (Bostock, 1970). The numerous valleys formed in the lowlands were shaped during the successive Pleistocene glaciations (Klassen, 1993). Since the Holocene, these valleys developed highly dynamic biogeosystems rich in permafrost ground ice, peat, and aquatic environments (Fortier and Allard, 2004). The study site (73°09′ N; 79°58′ W) is located in one such valley (glacier C-79) named Qarlikturvik, which has a NE–SW orientation and a surface area of ∼ 65 km^2 (∼ 15 km-long × 4–5 km-wide). A terminal moraine, located about halfway between the actual glacier front and the seashore and sitting on marine clay, was ^{14}C-dated to ∼ 9.8 kyr BP (Allard, 1996). Glacial retreat, accompanied by a marine transgression phase, ended around 6 kyr BP. The clays were then covered by glacio-fluvial sand and gravels (Fortier and Allard, 2004). Today, a proglacial braided river runs through a glacio-fluvial outwash plain and drains glacier melt waters and sediments towards the Navy Board Inlet, where it forms a delta.

The outwash plain is bordered on both sides by a 3 to 5 m-thick terrace, crisscrossed by networks of tundra polygons associated with the formation of syngenetic ice wedges (Figs. 1d and 2a). Along the southern bank of the river, the upper portion of the terrace is composed of alternating organic (peat) and mineral (wind-blown sand and silt) material, which started to accumulate over glacio-fluvial sands and gravels around 3700 years ago (Fortier and Allard, 2004). These peaty loess deposits contain excess pore ice (> 100 % dry weight) and their gravimetric organic matter content can reach over 50 %. The active layer depth in such deposits generally ranges between 40 to 60 cm, and the maximum depth of permafrost on Bylot Island has been estimated to be over 400 m (Smith and Burgess, 2000). The terrace comprises abundant aquatic

BGD
12, 11661–11705, 2015

systems of different sizes and shapes (Fig. 2) that can act as effective biogeochemical hotspots (Laurion et al., 2010; Negandhi et al., 2013). The hydrological network is mainly fed by rain and snowmelt runoff originating from gullies of the valley flanks or large snow banks on the lee side of hills. Most of water loss from ponds and lakes is through evaporation during the ice-free season (Negandhi, 2013).

The climate normal (1981–2010) is provided by a meteorological station located near the village of Pond Inlet (Mittimatalik) (72°41′ N; 77°58′ W), about 85 km southeast from the study site (Fig. 1c). The region has a polar climate with a slight marine influence, a mean annual air temperature of −14.6 °C (average daily temperatures ranging from −33.4 °C in January to 6.6 °C in July) and total precipitations of 189 mm, of which 91 mm fall as rain between June and September (Environment Canada, 2015). Thawing and freezing degree-days are around 475 and 5735, respectively. Winter (continuous daily mean air temperature < 0 °C) lasts from early September to mid-June, for an average total of 283 days year^{-1}. A station from the SILA network, operated since 2004 by the Center for Northern Studies (CEN) in the valley of glacier C-79, provides similar climate data. The mean annual air temperature over the last 10 years was −14.5 °C (with daily temperatures ranging from −34.7 °C in January to 6.2 °C in July), and total annual precipitations average 220 mm, of which 94 mm fall as rain (June to September) (CEN, 2014). Thawing and freezing degree-days range from ∼ 450 to 550 and from ∼ 4920 to 5670, respectively.

The southwest plain of Bylot Island is a ∼ 1600 km^2 low-lying wetland area of graminoid-moss tundra, which is an ideal nesting habitat for many migratory bird species such as Greater Snow Geese (Parks Canada, 2014). Local vegetation in the Qarlikturvik valley is dominated by sedges (e.g. *Carex aquatilis* var. *stans*, *Eriophorum scheuchzeri*), grasses (e.g. *Arctagrostis latifolia*, *Dupontia fischeri*, *Pleuropogon sabinei*) and mosses (e.g. *Drepanocladus* spp., *Aulocomnium* spp.) (Duclos, 2002; Ellis et al., 2008).

BGD
12, 11661–11705, 2015

3 Materials and methods

3.1 Sampling sites

We selected and sampled different types of aquatic systems typical of the tundra polygon terrace of the valley (Fig. 2; Table 1): (1) polygonal ponds over low-centered ice wedge polygons; (2) elongated water channels over melting ice wedges (ponds formed in collapsed ice-wedge troughs, hereafter referred to as trough ponds); (3) lakes with underlying talik (unfrozen soil over permafrost), including a thermokarst (thaw) lake and a kettle (melted buried glacier ice) lake. A total of 23 ponds and lakes were sampled in June–July 2013, including 9 polygonal ponds, 12 trough ponds, and 2 lakes (1 thermokarst and 1 kettle lake). In July 2014, six water bodies (two polygonal ponds, two trough ponds, and two lakes including one thermokarst and one kettle lake) were selected and studied more intensively, including morphological measurements of ponds (depth, width and length) and lakes (bathymetry with a portable sonar), and limnological profiles (see below).

3.2 Limnology

We measured a suite of limnological characteristics during both years, including temperature, dissolved oxygen, and concentrations of dissolved organic carbon (DOC), nutrients (phosphorus, nitrogen) and major ions. Temperature and dissolved oxygen profiles were recorded with a ProODO handheld meter (YSI Inc.). Water samples were filtered through 0.2 µm pre-rinsed cellulose acetate filters (2013) or pre-combusted GF/F filters (2014, nominal porosity 0.7 µm) to analyze DOC and major ions. Cations were fixed with HNO_3 (0.15 % final concentration) while anions and DOC were not fixed but kept in dark and cold. DOC concentrations were measured with a Shimadzu TOC-5000A carbon analyzer calibrated with potassium biphthalate. Major anions were quantified by ionic chromatography (Dionex ICS-2000), whereas major cations by inductively coupled plasma – optical emission spectrometry (ICP-OES, Varian VISTA

BGD
12, 11661–11705, 2015

AX). Total phosphorus (TP) and total nitrogen (TN) were quantified from unfiltered water samples fixed with H_2SO_4 (0.15 % final concentration) as described by Stainton et al. (1977).

3.3 Ebullition flux of greenhouse gases

Ebullition gas samples were collected using submerged funnels (as in Wik et al., 2013) equipped with a 140 mL plastic syringe (Fig. A1 in Appendix) and deployed for a period of 1 h to 19 days depending on the flux. The samples trapped in the syringe were transferred into 1–50 mL glass bottles with butyl rubber stoppers (bottles acid-washed, pre-combusted, helium flushed and vacuumed) for ^{14}C dating (see below), and 2–6 mL glass vials (helium flushed and vacuumed Exetainers) for stable isotope (see below) and gas chromatography analysis (Varian 3800 with a COMBI PAL head space injection system and a CP-Poraplot Q 25 m 3 0.53 mm column, flame ionization detector). Ebullition flux (F_e, in mmol m^{-2} d^{-1}) was calculated as:

$$F_e = (p_{Gas} \cdot V)/(A \cdot \mathrm{MV} \cdot t)$$

where p_{Gas} is the partial pressure of CO_2 or CH_4, V is the collected gas volume, A is the funnel area, MV is the gas molar volume at ambient air temperature, and t is the collecting time.

3.4 Diffusive flux of greenhouse gases

Surface water dissolved GHG concentrations were obtained by equilibrating 2 L of lake or pond water with 20 mL of ambient air during 3 min (Hesslein et al., 1991). The resulting gaseous headspace was transferred into 6 mL glass vials and analyzed as above by gas chromatography. Dissolved GHG concentration at the surface (C_{sur}) was calculated using Henry's law, and departure from saturation (sink vs. source) was calculated subtracting the gas concentration in the water at equilibrium with the atmosphere (C_{eq}, global values of atmospheric partial pressures from IPCC, 2007 were used). To

BGD
12, 11661–11705, 2015

estimate diffusive flux ($Flux_d$), first the gas transfer coefficient (k_{600}) standardized to a Schmidt number (Sc) of 600 (Wanninkhof, 1992) was calculated with the wind-based model of Cole and Caraco (1998):

$$k_{600} = 2.07 + 0.215u_{10}^{1.7}$$

where u_{10} is the wind speed at 10 m above the ground, and then applying the equation:

$$Flux_d = k(C_{sur} - C_{eq})$$

where k is the gas transfer coefficient for a given gas calculated as:

$$k = k_{600}(Sc/600)^{-0.5}$$

3.5 Radiocarbon analysis

Ebullition gas samples were analyzed at the Keck Carbon Cycle AMS facility at the University of California, Irvine. First, CH_4 and CO_2 were separated and purified by a zero air carrier gas flow-through line (Pack et al., 2015), and graphitized by the sealed tube Zn reduction method (Xu et al., 2007), then measured for radiocarbon (^{14}C) on a compact accelerator mass spectrometer (AMS) (Southon and Santos, 2007). Data presented here are expressed as $\Delta^{14}C$ (‰), which is normalized to radiocarbon activity of an oxalic acid standard OX1 (decay corrected to 1950) and corrected for isotopic fractionation (Reimer et al., 2004). $\Delta^{14}C$ (‰) > 0 was further used to indicate "modern" carbon (1950 to present), and $\Delta^{14}C$ (‰) < 0 for "older" carbon (pre-1950). This was particularly helpful for polygonal and trough ponds, which provided modern or very young GHG. The $\Delta^{14}C$ analytical error was ~ 2 ‰ for modern sample, based on long-term measurements of secondary standards. ^{14}C age (yr BP) is as defined by Stuiver and Polach (1977).

BGD
12, 11661–11705, 2015

3.6 Stable isotope analysis

Stable carbon and hydrogen isotopic compositions of GHG, $\delta^{13}CO_2$, $\delta^{13}CH_4$, and δDCH_4, were analyzed at the Biogeochemistry Facility School of Earth and Ocean Sciences (BF-SEOS, University of Victoria). Ebullition gas samples were analyzed for $\delta^{13}CH_4$ by introducing the gas onto a GSQ PLOT column (0.32 mm ID, 30 m) using a Valco 6-port valve and sample loop. After chromatographic separation, the CH_4 passes through an oxidation oven (1030 °C), a Nafion water trap, and open-split interface to a Continuous Flow-Isotope Ratio Mass Spectrometer (CF-IRMS). The $\delta^{13}CO_2$ was measured similarly by CF-IRMS, but bypassing the combustion oven. Precision for the $\delta^{13}CH_4$ and $\delta^{13}CO_2$ analyses was ±0.2 ‰, relative to Vienna PeeDee Belemnite (VPDB). Hydrogen isotope ratios of CH_4 (δDCH_4) were measured by a TC/EA pyrolysis unit (1450 °C) interfaced to a CF-IRMS. Precision for the δDCH_4 analyses was ±3 ‰, relative to Vienna Standard Mean Ocean Water (VSMOW). Carbon and hydrogen isotope ratios are expressed using standard delta (δ) notation as described by deviations from a standard such that:

$$\delta_{\text{sample}}‰ = [(R_{\text{sample}}/R_{\text{standard}}) - 1] \cdot 1000$$

where R is the $^{13}C/^{12}C$ or $^{2}H/^{1}H$ ratio in the sample or standard. For isotope calibration, methane carbon and hydrogen standards from Isometric Instruments were used. These are traceable back to VPDB for carbon isotope ratios and VSMOW for hydrogen isotope ratios.

4 Results

4.1 Morpho-limnological properties of ponds and lakes

Ponds were generally shallow (~ 0.6–0.8 m and 1.0–1.5 m deep for polygonal and trough ponds, respectively) and thus froze to the bottom during winter, whereas lakes

BGD
12, 11661–11705, 2015

were more variable in depth depending on their origin and at least a portion of them did not freeze to the bottom in winter. The thermokarst lake sampled was a few meters deep (< 5 m), while the kettle lake was deeper (< 12 m). Polygonal ponds, including different developmental stages and coalesced ponds, generally had flat bottoms covered by cyanobacterial mats (up to 5 cm thick), and stable (non eroding) shores (Fig. 2b and c). Their surface area varied substantially (from 21 to 3350 m^2) with a median of around 160 m^2. Trough ponds were elongated water channels (median width ~ 3 m; median length ~ 10 m), and their shores were either actively eroding with collapsing peat blocks (Fig. 2f), or stable and colonized by brown mosses (Fig. 2g). The thermokarst lake had sharp edges near the shore, a shallow and gently sloping lake bottom and a deeper central basin. The kettle lake had steeper slopes along its margins, and showed a deep section that was not in the center of the lake.

Ponds and lakes showed contrasting physicochemical conditions during the two sampling years (Table 1). Trough ponds generally had the highest concentrations of DOC, nutrients and ions, followed by polygonal ponds, whereas lakes showed the lowest values. Trough pond BYL27, where shore erosion was active during summer time, had near- or higher-than-average concentrations, whereas trough pond BYL24, with stable shores, showed lower-than average values. Pond DOC, nutrient and ion concentrations were substantially higher in 2014, a particularly dry year (total precipitations from January to June = 27.0 mm in 2014, compared to 50.7 mm in average; Table B1 in Appendix), with resulting low pond water levels as observed in the field.

Polygonal ponds (BYL30, BYL80) had a thermally homogenous and well-oxygenated water column in July, whereas trough ponds (BYL24, BYL27) were notably stratified (Fig. 3). Thermokarst lake BYL66 was relatively well mixed over most of the water column, except near the sediment–water interface where dissolved oxygen decreased rapidly. Kettle lake BYL36, deeper than the other sampled water bodies, showed a steep gradient between the warmer, well-oxygenated epilimnion and the much colder, anoxic hypolimnion.

BGD
12, 11661–11705, 2015

4.2 Age and concentration of greenhouse gases released through ebullition

Radiocarbon age ($\Delta^{14}C$ signature) and concentration of GHG (CO_2 and CH_4) emitted through ebullition showed strikingly different trends between the various types of aquatic systems (Fig. 4). Polygonal and trough ponds produced modern CH_4 and modern to a few hundred years old (< 550 yr BP) CO_2, whereas lakes generally released older GHG, ranging from 510 to 1425 yr BP for CO_2 and from 125 to 3405 yr BP for CH_4 (Table 2). Moreover, samples from lake edges had younger and less concentrated CH_4 than those coming from lake central area. No such trend was observed for CO_2 in lakes. Considering all ponds and lakes as a whole, CH_4 was generally one to two orders of magnitude more concentrated than CO_2 in emitted bubbles in July, with median partial pressure of 3.3×10^5 ppmv (range 2.7×10^4–4.7×10^5 ppmv) for CH_4 and $\sim 5.0 \times 10^3$ ppmv (range 7.7×10^2–3.1×10^4 ppmv) for CO_2.

4.3 Dissolved and ebullition fluxes of greenhouse gases

Polygonal ponds were generally CO_2 sinks, but they were CH_4 sources with a relatively broad range of saturation levels ($\sim$ 0–2.4 µM) (Fig. 5). Lakes were near the equilibrium with the atmosphere (all samples clustered near 0 for both gases), being small sinks or sources of CO_2, and small sources of CH_4. Trough ponds were in general supersaturated in both gases, especially when their margins were actively eroding (highest GHG saturation values) (Fig. C1). Trough ponds showed the highest diffusive flux, especially of CO_2 (65.5 mmol m^{-2} d^{-1}; Table 3) with a median diffusive CO_2 flux (21.8 mmol m^{-2} d^{-1}) more than 12 times higher than the median value of all sampled water bodies (1.7 mmol m^{-2} d^{-1}). Polygonal ponds, on the other hand, showed the highest ebullition flux for both CO_2 (16.3 mmol m^{-2} d^{-1}) and CH_4 (534.5 mmol m^{-2} d^{-1}), with a median ebullition CH_4 flux that, although relatively low ($\sim$ 1.0 mmol m^{-2} d^{-1}), was $\sim$ 5 times higher than the median value for all ponds and lakes ($\sim$ 0.2 mmol m^{-2} d^{-1}). Lakes generally showed the lowest fluxes (both diffusion and ebullition). Globally, dif-

BGD
12, 11661–11705, 2015

fusion appeared as the dominant mechanism for CO_2 emission, whereas CH_4 was mainly emitted through ebullition.

4.4 Carbon and hydrogen stable isotope ratios in ebullition gas samples

The stable isotope ratios of methane ($\delta^{13}CH_4$, δDCH_4) and carbon dioxide ($\delta^{13}CO_2$) were measured on 18 ebullition samples collected in 2013 and 2014 (Table 2). The $\delta^{13}CH_4$ average values were −60.5 ‰ and ranged from −52.1 ‰ to the most ^{13}C-depleted value of −67.6 ‰, both from polygonal ponds. The δDCH_4 values, which averaged −376.80 ‰, were relatively ^{2}H-depleted for naturally occurring methane. The δDCH_4 with the most ^{2}H-enriched value came from the thermokarst lake sample (−319.56 ‰; BYL66). In contrast, the δDCH_4 values from trough ponds (BYL24 and BYL27) were consistently and extremely ^{2}H-depleted, with values from −397.7 ‰ to a very low value of −448.1 ‰. There was no apparent correspondence between the methane concentration and $\delta^{13}CH_4$ or δDCH_4. The CO_2 contents of ebullition samples were sometimes insufficient for carbon isotope measurements. For those with more CO_2, the average $\delta^{13}CO_2$ was −14.3 ‰ and varied from +0.3 to −21.8 ‰. There was also no apparent correspondence between the CO_2 concentration and $\delta^{13}CO_2$. However, it is worth noting that the sample with the most ^{13}C-enriched CO_2 also corresponded to the one with the most ^{13}C-depleted CH_4 (polygonal pond BYL80).

5 Discussion

5.1 The strong heterogeneity in greenhouse gas age and concentration

Our results showed large variability in limnological properties of ponds and lakes, as well as in the age and concentration of carbon processed and ultimately released as GHG by these aquatic systems. The GHG escaping through ebullition ranged from modern to a few centuries old for polygonal and trough ponds, and from a few centuries

BGD
12, 11661–11705, 2015

to a few millennia old for lakes (Fig. 4). We found that trough ponds emitted slightly but significantly older CH_4 than polygonal ponds ($\Delta^{14}C = 10 \pm 18$ vs. 43 ± 28 ‰, respectively; $p < 0.05$) such as observed earlier at the same site (Negandhi et al., 2013), indicating a small contribution of peat-derived carbon pool to microbial activity. Most surprisingly however, trough ponds did not emit (millennium-) old CH_4, at least in July, despite the fact that they were exposed to eroding peat from down to the base of the active layer in the surroundings (^{14}C dates ranging from ~ 2.2 to 2.5 k yr BP; Table 2) and older peaty strata up-thrusted along ice wedges during their growth and now reaching the ridges' surface (Fortier and Allard, 2004). Eroding peat was likely leaching old carbon into the water column, but bottom sediment interstitial water, where CH_4 is mostly produced, did not predominantly emit carbon of this age. Permafrost disturbance was indeed shown to deliver millennia-old particulate organic carbon and DOC to arctic streams and rivers (Lamoureux and Lafrenière, 2014; Guo et al., 2007; Vonk et al., 2013). We speculate that microbes are preferably using young (putatively more labile) carbon in thaw ponds at this time of the year, and may use the older carbon stocks later when primary producers are less active. If the CH_4 released from trough ponds is indeed older during the following autumn and spring, it would have large implications on the role of such ponds as a positive feedback mechanism on climate.

On the other hand, CH_4 ebullition samples collected from lakes provided older dates, up to nearly 3500 yr BP (thermokarst lake BYL66), which is very close to the maximum known age of the permafrost peat layers in the valley (3670 ± 110 yr BP; Fortier and Allard, 2004). It may suggest that permafrost thaw underneath this lake have proceeded through the organic layers at this site, which could result in decreased emissions in the future after the microbial exhaustion of the labile fraction of the organic matter pool (Walter et al., 2007). However the timing of this reduction is unknown. We observed a spatial gradient in the age and concentration of CH_4 in bubbles emitted from the thermokarst lake, with younger and less concentrated CH_4 from the lake edge (~ 3 %), and older and more concentrated CH_4 from the center (up to 44 %). The development of a talik (unfrozen soil under lake) explains the mobilization of deeper and older CH_4

BGD
12, 11661–11705, 2015

at the lake center where water remains unfrozen under the ice cover in winter (maximum lake depth > 4 m, ice cover thickness ~ 2 m). Methane emitted from a given area of the lake would thus be composed of a mixing of young CH_4 from the edge with older CH_4 from the center, with a ^{14}C signature of source $\sim -360 \pm 18$ ‰, corresponding to > 3500 yr BP (when using the 2014 data ; Fig. D1). To our knowledge, the only other studies of thermokarst lakes presenting ^{14}C dates on GHG are in *yedoma* regions (Alaska, Siberia), which have a very different ground ice, sediment and carbon stocks, and chronostratigraphic history. For these lakes, the release of very old (> 40 k yr BP) and highly concentrated (up to 90 %) CH_4 from deep unfrozen lake sediments has been found (Walter et al., 2008). However, this study also reported younger ages for ebullition samples emitted from different parts of the lakes, generally younger towards the lake center (background ebullition). At our study site, even though older GHG were emitted from lakes compared to ponds, ebullition fluxes remained low during the study period (July). Walter-Anthony and Anthony (2013) concluded that the classic randomized bubble-trap method for estimating mean lake ebullition is highly median-biased toward underestimation of fluxes, and this was possibly also occurring for our data set although no systematic GHG point source studies have been conducted so far at our study site.

We also observed strong differences in dissolved GHG flux depending on pond and lake types (Fig. 5; Table 3): polygonal ponds were CO_2 sinks but CH_4 sources, trough ponds were significant sources of both GHG as previously reported in the valley (Laurion et al., 2010; Negandhi et al., 2013), and lakes were small sources of GHG. This can be explained by their morpho-limnological properties. Polygonal ponds had stabilized shores (no apparent slumping) and more transparent waters compared to other systems, as shown by their lower colored dissolved organic matter (CDOM) content (Laurion et al., 2010). Moreover, they had flat and shallow bottoms covered by abundant cyanobacterial mats actively photosynthesizing and acting as an efficient CO_2 sink (flux reaching $-11.8\,mmol\,m^{-2}\,d^{-1}$). Bottom sediments of these ponds were also colonized by methanotrophic bacteria (Negandhi et al., 2014), which can be a signifi-

BGD
12, 11661–11705, 2015

cant control mechanism on CH_4 emissions such as shown in polygonal tundra ponds of the Lena region (Liebner et al., 2011).

Lakes were larger and deeper, thus they were exposed to wind-induced mixing of their epilimnetic waters promoting venting of the GHG from this layer. When the water column is seasonally stratified (like in BYL36), the hypolimnion likely stores a large fraction of the GHG produced by the lake until the autumnal overturn period (Bastviken et al., 2004), allowing more space and time for the oxidation of dissolved CH_4, and for the dissolution of a fraction of ebullition CH_4 (Bastviken et al., 2008). Therefore, it is possible that higher flux of old carbon would be observed later in the season. To fully account GHG emissions from lakes and compare them to other aquatic systems, summer and winter storage fluxes will need to be estimated (Boereboom et al., 2012; Langer et al., 2015; Walter Anthony et al., 2010; Wik et al., 2011).

Trough ponds presented the highest GHG fluxes. Despite their shallow depths, they were strongly stratified with oxygen-depleted bottom waters, and were not colonized by photosynthesizing (CO_2 sink) and methanotrophic (CH_4 sink) bacteria such as in polygonal ponds (Negandhi et al., 2014). Stronger water column hypoxia generated anoxia more rapidly in the sediments, and the organic material inputs caused by active erosion likely led to higher CH_4 production (BYL27). Meanwhile, the unstable conditions and reduced light availability (higher CDOM, TP and turbidity; Table 1) favored net heterotrophy (CO_2 emissions). Similar to polygonal ponds, the shallow depth of trough ponds reduces the chances for dissolution of CH_4 bubbles into the water column and its subsequent oxidation before reaching the atmosphere. Moreover, the thermal structure of trough ponds, linked to their low transparency to solar energy and to the surrounding microtopography reducing wind turbulent energy, can impede mixing for several weeks (Fig. 6), thus favoring GHG storage in bottom waters in July, and stronger diffusive fluxes later in the season during water column mixing. Thermal structure might become even stronger in years of low precipitations such as in 2014, when concentrations of solutes (DOC, ions) increase through evaporation, intensifying density gradients thus GHG storage.

BGD
12, 11661–11705, 2015

The highest GHG saturation levels observed over the sampling period were measured in a trough pond the day following a major erosion event (peat block collapsing in pond BYL27, Fig. C1). This might result from the disturbance of the thermal structure and transfer of stored GHG to the surface, or from the causal effect of a new input of organic matter to microbial activity. Active shore erosion around tundra ponds, potentially increasing CH_4 production by 2 to 3 orders of magnitude, has been reported from similar systems in Siberia (Langer et al., 2015), suggesting a direct impact of permafrost slumping on GHG emissions. The effect of erosion events on GHG flux must be further evaluated as other factors, such as fluctuating meteorological conditions (e.g., wind orientation along trough axis, major changes in air temperature and its effect on heat exchange; Tedford et al., 2014) can also influence mixing and surface GHG concentrations.

Interestingly, we also observed substantial differences in GHG concentrations among trough ponds, some presenting much lower values. Trough ponds such as BYL24 (Fig. 2g) had relatively stable (non eroding) shores, and were colonized by abundant vegetation dominated by brown mosses. Methane oxidation by bacteria associated with submerged brown mosses has been reported in Siberian ponds, contributing to smaller CH_4 concentrations in these ecosystems (Liebner et al., 2011). Therefore, there might be cases where the methanotrophic community is also efficient in limiting CH_4 emissions from trough ponds (Negandhi et al., 2014).

5.2 Production pathways of CO_2 and CH_4

We obtained different radiocarbon ages for CO_2 and CH_4 within the same ebullition samples, as collected from funnels placed at the water surface (Table 2, Fig. 4), suggesting that GHG production was derived by different carbon sources. This divergence in carbon age was even more pronounced for the lakes, where it could reach almost 3000 years. The presence of unfrozen sediment layers (talik) underneath the lakes would explain the older bubbling CH_4 emitted from deeper/older sediments exposed to microbial degradation, such as found in thermokarst lakes of Siberia and Alaska

BGD
12, 11661–11705, 2015

(Walter et al., 2007). Younger CO_2 could then be explained by a larger contribution of younger and shallower surface sediments to bacterial consumption. It could also result from lateral inputs of CO_2 produced by younger organic material or from exchanges with atmospheric CO_2.

On the other hand, century-old CO_2 collected from ponds in parallel to modern CH_4 is more difficult to explain. As stated above, emission of young CH_4 suggests the preferential use of modern carbon by methanogens and a dominance of background ebullition mode (from surface sediments) in thaw ponds. Meanwhile, emission of older CO_2 could be related to anaerobic CO_2 production in water-saturated and reductive soils and its subsequent lateral transport, as observed in a flooded tundra site in Alaska (Zona et al., 2012). Characterizing organic matter properties and oxidation *vs.* reduction (redox) potential of pond and lake sediments at our study sites are required to confirm if such a mechanism can contribute to modern CH_4 emissions from surface layers and, at the same time, older CO_2 emissions from deeper layers. Moreover, a quantification of lateral fluxes of carbon within active layer groundwater, an important yet rarely mentioned process driven by the coupling between carbon and water cycles (Vonk and Gustafsson, 2013; Paytan et al., 2015), could help to better understand these results.

Notwithstanding the above-mentioned differences, the concentrations of CO_2 and CH_4 emitted through ebullition also need to be taken into account when evaluating the climate feedback role of these emissions. Even though the age of CO_2 could reach several centuries (> 1000 yr BP for one sample; Fig. 4), it was one to two orders of magnitude less concentrated in the emitted bubbles than CH_4. Therefore, considering ice-free season ebullition, only CH_4 has the potential to act as a positive feedback mechanism. Similar observations were reported from Siberian lakes, despite notably different geomorphological, geocryological and limnological conditions (Walter et al., 2007).

Methanogenesis in cold wetland systems typically proceeds via the anaerobic fermentation pathways of acetoclastic methanogenesis (AM) and/or hydrogenotrophic carbonate reduction methanogenesis (HM) (e.g., Kotsyurbenko et al., 2004; Alstad and

BGD
12, 11661–11705, 2015

Whiticar, 2011). AM utilizes the transfer of a CH_3^- group from preformed organic substrates (i.e., acetate, methanol, methylated substrates, etc.), whereas HM utilizes H_2 and CO_2. Numerous studies have demonstrated the ability of using methane C and H isotope signatures to discriminate AM from HM pathways, and to characterize secondarily altered methane (oxidation, mixing, etc.). Polygonal ponds and lakes had combined methane C and H stable isotope signatures that were typical for methanogenesis dominated by AM, as strongly illustrated in the plot of $\delta^{13}CH_4$ vs. δDCH_4 (Fig. 7). Trough ponds shared similar $\delta^{13}CH_4$ values with the other water bodies, but had substantially more ^{2}H-depleted values (δDCH_4 from −398 to −448 ‰; Table 2, Fig. 7). These values are among the most ^{2}H-depleted values known for naturally occurring methane (e.g., Whiticar, 1999). Although there was some variation between sites, the isotope signatures designate that all CH_4 emitted by ebullition during the summer is produced by AM, consistent with an earlier study at the same site (Negandhi et al., 2013). There is no indication of HM, which has a very different isotope signature. This finding of AM dominance is consistent with ombrotrophic bogs with higher pH (ranging from ∼ 6.7 to 10.0, measured in 2014 using a YSI) compared with more acidic minerotrophic wetlands, which can be HM dominated (e.g., Bowes and Hornibrook, 2006; Prater et al., 2007). The dominance of AM is likely related to the carbon precursors. Our sites may have more labile organic material present (e.g., organic acids) supporting acetoclastic methanogenesis and recently made available to methanogens. As this labile carbon pool is exhausted, the methanogenic pathway shifts from acetoclastic to more recalcitrant compounds and hence hydrogenotrophic methanogenesis (e.g., Alstad and Whiticar, 2011).

Previous work in this valley indicated a significant relationship between water oxygen concentration and dissolved CH_4 oxidation level (Negandhi et al., 2013). This work also showed evidence that diffusive CH_4 was more susceptible to oxidation in polygonal ponds where a methanotrophic community was favored (Negandhi et al., 2014). This conclusion was supported by the strong shift in $\delta^{13}CH_4$ and δDCH_4 to the heavier isotopes, as expected (Whiticar et al., 1986). In the present study, there was no evidence

BGD
12, 11661–11705, 2015

of methane oxidation in any of the collected ebullition samples (Fig. 8), indicating that the conditions did not favor oxidation at the production site (likely in anoxic sediment but also potentially in the water column; Grossart et al., 2011), and that the exchange with a pool of oxidized methane during the transport of bubbles to surface waters was undetectable, possibly linked to the short residence time. This was expected for shallow waters where bubbles can rapidly escape, but it was also the case in larger and deeper stratified lakes such as BYL36.

5.3 Bylot ponds and lakes within the circumpolar North

The general topography and geology of the Bylot southwest plain, together with the distinct local conditions of the Qarlikturvik valley (e.g., glacier and outwash plain activity, valley orientation in relation to dominant winds, snow cover depth and density), have contributed to the development over thousands of years of what is arguably one of the richest ecosystems in the region. However, taken separately, most of the landscape features in the valley (e.g., tundra polygons, ice-wedges, thermokarst ponds and lakes) are widespread across the Arctic (e.g., Walter Anthony et al., 2010; Abnizova et al., 2012; Langer et al., 2015). When compared with flux values reported in the literature, our results, representing a snapshot of mid-summer conditions, generally appear in the range of what has been observed in other ponds and lakes from northern regions (Table 4). For example, we measured total CO_2 fluxes (diffusion + ebullition) of up to $\sim 0.8\,g\,C\,m^{-2}\,d^{-1}$, which is in the range of those reported from Alaska (0.7–$2.3\,g\,C\,m^{-2}\,d^{-1}$; Kling et al., 1992; Sepulveda-Jauregui et al., 2014), Siberia (0.02–$1.1\,g\,C\,m^{-2}\,d^{-1}$; Abnizova et al., 2012; Blodau et al., 2008), and Scandinavia (0.9–$1.6\,g\,C\,m^{-2}\,d^{-1}$; Huttunen et al., 2003; Kankaala et al., 2013). Methane fluxes (diffusion + ebullition) at our study site varied substantially ($0.0005–6.4\,g\,C\,m^{-2}\,d^{-1}$), but could reach values one order of magnitude higher than those from lakes in Alaska (0.01–$0.5\,g\,C\,m^{-2}\,d^{-1}$; Kling et al., 1992; Sepulveda-Jauregui et al., 2014; Walter Anthony and Anthony, 2013) and Scandinavia ($0.01–0.1\,g\,C\,m^{-2}\,d^{-1}$; Bastviken et al., 2004; Huttunen et al., 2003; Kankaala et al., 2013). However, median values for polygonal and

BGD
12, 11661–11705, 2015

trough ponds (~ 0.02 and 0.01 g C m^{-2} d^{-1}, respectively) were more similar to published ranges. Yet, these fluxes were lower than those reported from Siberian thermokarst lakes in *yedoma* deposits (nearly 20 g C m^{-2} d^{-1}; Walter Anthony et al., 2010), which however include discrete ebullition seeps and hotspots that were not observed in our study, and most likely do not exist in the case of ponds.

6 Conclusions

Aquatic systems are widespread across permafrost landscapes and play a crucial role in large-scale biogeochemical cycles. Yet, there is still much uncertainty about whether or not the Arctic can globally be considered a carbon source or sink. One element of such uncertainty is the highly heterogeneous distribution of ponds and lakes at the local scale and their different geomorphological and limnological properties, which influence their biogeochemistry and result in highly variable fluxes from these waters, especially for trough ponds. Our study demonstrates that local geomorphology and shoreline erosion around permafrost thaw ponds and lakes can have a strong impact on their GHG concentrations and fluxes. We also report substantially different GHG ages among ponds and lakes of contrasting sizes and depths, and unexpectedly the emission of mainly modern CH_4 from trough ponds despite their exposure to a stock of eroding old carbon. Such results underscore the importance of the combined effects of geomorphology (thaw bulb development level), limnology (CH_4 production and storage in anoxic/hypoxic bottom waters) and hydrology (lateral runoff inputs of organic material or GHG) on GHG emissions by permafrost thaw ponds and lakes. The dominance of acetoclastic methanogenesis in these environments indicates that the system is rich in labile precursor substrates (e.g., acetate, formate, methylated substrates). Finally, the oldest CH_4 ages (~ 3.5 k yr BP) obtained from a thermokarst lake corresponded to the maximal age of the frozen organic (peat) layers in the valley, suggesting that permafrost thaw might have (or will soon have) proceeded through the organic substrate

BGD
12, 11661–11705, 2015

at this site. Such lakes covered a smaller area in the valley than small and shallow ponds, which provided most of the observed GHG emissions, mainly of a modern age.

The Supplement related to this article is available online at doi:10.5194/bgd-12-11661-2015-supplement.

Author contributions. F. Bouchard, I. Laurion and V. Prėskienis designed the experiments, and F. Bouchard and V. Prėskienis performed them. I. Laurion, D. Fortier, X. Xu and M. J. Whiticar contributed materials, instruments and analyses. F. Bouchard, I. Laurion, V. Prėskienis and D. Fortier analyzed the data. F. Bouchard prepared the manuscript with contributions from all co-authors.

Acknowledgements. We are grateful to H. White, G. Lupiens, D. Sarrazin and the team of G. Gauthier (U. Laval) for their help on the field, and to S. Duval, A. Bensadoune and J. F. Dutil for their help in the laboratory. We also thank the Pond Inlet (Mittimatalik) community, the Center for Northern Studies (CEN) and Parks Canada (Sirmilik National Park) for logistical support and access to the study site. This project was funded by ArcticNet, the Natural Sciences and Engineering Research Council of Canada (NSERC), the Polar Continental Shelf Program (PCSP) of Natural Resources Canada, the NSERC Discovery Frontiers grant "Arctic Development and Adaptation to Permafrost in Transition" (ADAPT), the EnviroNorth Training Program, and the W. Garfield Weston Foundation.

References

Abnizova, A., Siemens, J., Langer, M., and Boike, J.: Small ponds with major impact: the relevance of ponds and lakes in permafrost landscapes to carbon dioxide emissions, Global Biogeochem. Cy., 26, GB2041, doi:10.1029/2011gb004237, 2012.

Allard, M.: Geomorphological changes and permafrost dynamics: key factors in changing arctic ecosystems. An example from Bylot Island, Nunavut, Canada, Geosci. Can., 23, 205–212, 1996.

BGD
12, 11661–11705, 2015

Alstad, K. P. and Whiticar, M. J.: Carbon and hydrogen isotope ratio characterization of methane dynamics for fluxnet peatland ecosystems, Org. Geochem., 42, 548–558, doi:10.1016/j.orggeochem.2011.03.004, 2011.
Bastviken, D., Cole, J., Pace, M., and Tranvik, L.: Methane emissions from lakes: dependence of lake characteristics, two regional assessments, and a global estimate, Global Biogeochem. Cy., 18, GB4009, doi:10.1029/2004GB002238, 2004.
Bastviken, D., Cole, J. J., Pace, M. L., and Van de Bogert, M. C.: Fates of methane from different lake habitats: connecting whole-lake budgets and CH_4 emissions, J. Geophys. Res.-Biogeo., 113, G02024, doi:10.1029/2007jg000608, 2008.
Blodau, C., Rees, R., Flessa, H., Rodionov, A., Guggenberger, G., Knorr, K. H., Shibistova, O., Zrazhevskaya, G., Mikheeva, N., and Kasansky, O. A.: A snapshot of CO_2 and CH_4 evolution in a thermokarst pond near Igarka, northern Siberia, J. Geophys. Res.-Biogeo., 113, G03023, doi:10.1029/2007jg000652, 2008.
Boereboom, T., Depoorter, M., Coppens, S., and Tison, J.-L.: Gas properties of winter lake ice in Northern Sweden: implication for carbon gas release, Biogeosciences, 9, 827–838, doi:10.5194/bg-9-827-2012, 2012.
Bostock, H. S.: Physiographic subdivisions of Canada, in: Geology and Economic Minerals of Canada. Economic Geology Report No. 1, edited by: Douglas, R. J. W., Geological Survey of Canada, Ottawa, 9–30, 1970.
Bowes, H. L. and Hornibrook, E. R. C.: Emission of highly ^{13}C-depleted methane from an upland blanket mire, Geophys. Res. Lett., 33, L04401, doi:10.1029/2005GL025209, 2006.
Brosius, L. S., Walter Anthony, K. M., Grosse, G., Chanton, J. P., Farquharson, L. M., Overduin, P. P., and Meyer, H.: Using the deuterium isotope composition of permafrost meltwater to constrain thermokarst lake contributions to atmospheric CH_4 during the last deglaciation, J. Geophys. Res.-Biogeo., 117, G01022, doi:10.1029/2011jg001810, 2012.
Brown, J., Ferrians, O. J., Heginbottom, J. A., and Melnikov, E. S.: Circum-Arctic Map of Permafrost and Ground-Ice Conditions, National Snow and Ice Data Center/World Data Center for Glaciology, Boulder, Colorado, 1998.
Burn, C. R. and Kokelj, S. V.: The environment and permafrost of the Mackenzie Delta area, Permafrost Periglac., 20, 83–105, doi:10.1002/ppp.655, 2009.
CEN: Environmental Data from Bylot Island in Nunavut, Canada, v. 1.4 (1992–2014), Nordicana D2, doi:10.5885/45039SL-EE76C1BDAADC4890 (last access: 20 March 2015), 2014.

BGD
12, 11661–11705, 2015

Cole, J. J. and Caraco, N. F.: Atmospheric exchange of carbon dioxide in a low-wind oligotrophic lake measured by the addition of SF_6, Limnol. Oceanogr., 43, 647–656, 1998.
Duclos, I.: Milieux mésiques et secs de l'île Bylot, Nunavut (Canada): caractérisation et utilisation par la grande oie des neiges, MSc thesis, Université du Québec à Trois-Rivières (UQTR), 115 pp., 2002.
Dyke, A. S. and Prest, V. K.: Late Wisconsinan and Holocene History of the Laurentide Ice Sheet, Geogr. Phys. Quatern., 41, 237–263, 1987.
Ellis, C. J., Rochefort, L., Gauthier, G., and Pienitz, R.: Paleoecological evidence for transitions between contrasting landforms in a polygon-patterned High Arctic wetland, Arct. Antarct. Alp. Res., 40, 624–637, doi:10.1657/1523-0430(07-059)[ellis]2.0.co;2, 2008.
Environment Canada: 1981–2010 Climate Normals & Averages, available at: http://climate.weather.gc.ca/climate_normals/index_e.html (last access: 10 February 2015), 2015.
Fortier, D. and Allard, M.: Late Holocene syngenetic ice-wedge polygons development, Bylot Island, Canadian Arctic Archipelago, Can. J. Earth Sci., 41, 997–1012, doi:10.1139/e04-031, 2004.
Fortier, D., Allard, M., and Pivot, F.: A late-Holocene record of loess deposition in ice-wedge polygons reflecting wind activity and ground moisture conditions, Bylot Island, eastern Canadian Arctic, Holocene, 16, 635–646, doi:10.1191/0959683606hl960rp, 2006.
Gao, X., Schlosser, C. A., Sokolov, A., Walter Anthony, K. W., Zhuang, Q. L., and Kicklighter, D.: Permafrost degradation and methane: low risk of biogeochemical climate-warming feedback, Environ. Res. Lett., 8, 035014, doi:10.1088/1748-9326/8/3/035014, 2013.
Godin, E., Fortier, D., and Coulombe, S.: Effects of thermo-erosion gullying on hydrologic flow networks, discharge and soil loss, Environ. Res. Lett., 9, 105010, doi:10.1088/1748-9326/9/10/105010, 2014.
Grossart, H.-P., Frindte, K., Dziallas, C., Eckert, W., and Tang, K. W.: Microbial methane production in oxygenated water column of an oligotrophic lake, P. Natl. Acad. Sci. USA, 108, 19657–19661, doi:10.1073/pnas.1110716108, 2011.
Grosse, G., Jones, B., and Arp, C.: Thermokarst lakes, drainage, and drained basins, in: Treatise on Geomorphology, Glacial and Periglacial Geomorphology, 8, edited by: Shroder, J. F., Academic Press, San Diego, CA, 325–353, 2013.
Guo, L., Ping, C.-L., and Macdonald, R. W.: Mobilization pathways of organic carbon from permafrost to arctic rivers in a changing climate, Geophys. Res. Lett., 34, L13603, doi:10.1029/2007GL030689, 2007.

BGD
12, 11661–11705, 2015

Hesslein, R. H., Rudd, J. W. M., Kelly, C. A., Ramlal, P., and Hallard, K. A.: Carbon dioxide pressure in surface waters of Canadian lakes, in: Air-Water Mass Transfer, edited by: Wilhelms, S. C. and Gulliver, J. S., American Society of Civil Engineers, New York, 413–431, 1991.

Hugelius, G., Strauss, J., Zubrzycki, S., Harden, J. W., Schuur, E. A. G., Ping, C.-L., Schirrmeister, L., Grosse, G., Michaelson, G. J., Koven, C. D., O'Donnell, J. A., Elberling, B., Mishra, U., Camill, P., Yu, Z., Palmtag, J., and Kuhry, P.: Estimated stocks of circumpolar permafrost carbon with quantified uncertainty ranges and identified data gaps, Biogeosciences, 11, 6573–6593, doi:10.5194/bg-11-6573-2014, 2014.

Huttunen, J. T., Alm, J., Liikanen, A., Juutinen, S., Larmola, T., Hammar, T., Silvola, J., and Martikainen, P. J.: Fluxes of methane, carbon dioxide and nitrous oxide in boreal lakes and potential anthropogenic effects on the aquatic greenhouse gas emissions, Chemosphere, 52, 609–621, doi:10.1016/S0045-6535(03)00243-1, 2003.

IPCC: Changes in Atmospheric Constituents and in Radiative Forcing, in: Climate Change 2007: The Physical Science Basis. Contribution of Working Group I to the Fourth Assessment Report of the Intergovernmental Panel on Climate Change, edited by: Solomon, S., Qin, D., Manning, M., Chen, Z., Marquis, M., Averyt, K. B., Tignor, M., and Miller, H. L., Cambridge University Press, Cambridge, UK, 129–234, 2007.

Kankaala, P., Huotari, J., Tulonen, T., and Ojala, A.: Lake-size dependent physical forcing drives carbon dioxide and methane effluxes from lakes in a boreal landscape, Limnol. Oceanogr., 58, 1915–1930, doi:10.4319/lo.2013.58.6.1915, 2013.

Klassen, R. A.: Quaternary Geology and Glacial History of Bylot Island, Northwest Territories, Geological Survey of Canada, Ottawa, 1993.

Kling, G. W., Kipphut, G. W., and Miller, M. C.: The flux of CO_2 and CH_4 from lakes and rivers in arctic Alaska, Hydrobiologia, 240, 23–36, doi:10.1007/bf00013449, 1992.

Kotsyurbenko, O. R., Chin, K.-J., Glagolev, M. V., Stubner, S. Simankova, M. V., Nozhevnikova, A. N., and Conrad, R.: Acetoclastic and hydrogenotrophic methane production and methanogenic populations in an acidic West-Siberian peat bog, Environ. Microbiol., 6, 1159–1173, doi:10.1111/j.1462-2920.2004.00634.x, 2004.

Lamoureux, S. F. and Lafrenière, M. J.: Seasonal fluxes and age of particulate organic carbon exported from Arctic catchments impacted by localized permafrost slope disturbances, Environ. Res. Lett., 9, 045002, doi:10.1088/1748-9326/9/4/045002, 2014.

BGD
12, 11661–11705, 2015

Langer, M., Westermann, S., Walter Anthony, K., Wischnewski, K., and Boike, J.: Frozen ponds: production and storage of methane during the Arctic winter in a lowland tundra landscape in northern Siberia, Lena River delta, Biogeosciences, 12, 977–990, doi:10.5194/bg-12-977-2015, 2015.

Lauriol, B., Lacelle, D., St-Jean, M., Clark, I. D., and Zazula, G. D.: Late Quaternary paleoenvironments and growth of intrusive ice in eastern Beringia (Eagle River Valley, northern Yukon, Canada), Can. J. Earth Sci., 47, 941–955, doi:10.1139/e10-012, 2010.

Laurion, I., Vincent, W. F., MacIntyre, S., Retamal, L., Dupont, C., Francus, P., and Pienitz, R.: Variability in greenhouse gas emissions from permafrost thaw ponds, Limnol. Oceanogr., 55, 115–133, doi:10.4319/lo.2010.55.1.0115, 2010.

Liebner, S., Zeyer, J., Wagner, D., Schubert, C., Pfeiffer, E. M., and Knoblauch, C.: Methane oxidation associated with submerged brown mosses reduces methane emissions from Siberian polygonal tundra, J. Ecol., 99, 914–922, doi:10.1111/j.1365-2745.2011.01823.x, 2011.

Negandhi, K.: Defining water sources and extent of evaporation of arctic thermokarst (thaw) ponds using water isotope tracers, Scientific and Technical Document No. I357, Institut National de la Recherche Scientifique (INRS), Centre Eau Terre Environnement (ETE), Québec City, 2013.

Negandhi, K., Laurion, I., Whiticar, M. J., Galand, P. E., Xu, X., and Lovejoy, C.: Small thaw ponds: an unaccounted source of methane in the Canadian High Arctic, Plos One, 8, e78204, doi:10.1371/journal.pone.0078204, 2013.

Negandhi, K., Laurion, I., and Lovejoy, C.: Bacterial communities and greenhouse gas emissions of shallow ponds in the High Arctic, Polar Biol., 37, 1669–1683, doi:10.1007/s00300-014-1555-1, 2014.

Pack, M. A., Xu, X., Lupascu, M., Kessler, J. D., and Czimczik, C. I.: A rapid method for preparing low volume CH_4 and CO_2 gas samples for ^{14}C AMS analysis, Org. Geochem., 78, 89–98, doi:10.1016/j.orggeochem.2014.10.010, 2015.

Parks Canada: Sirmilik National Park of Canada, available at: http://www.pc.gc.ca/eng/pn-np/nu/sirmilik/index.aspx (last access: 10 February 2014), 2014.

Paytan, A., Lecher, A. L., Dimova, N., Sparrow, K. J., Kodovska, F. G.-T., Murray, J., Tulaczyk, S., and Kessler, J. D.: Methane transport from the active layer to lakes in the Arctic using Toolik Lake, Alaska, as a case study, P. Natl. Acad. Sci. USA, 112, 3636–3640, doi:10.1073/pnas.1417392112, 2015.

BGD
12, 11661–11705, 2015

Prater, J. L., Chanton, J. P., and Whiting, G. J.: Variation in methane production pathways associated with permafrost decomposition in collapse scar bogs of Alberta, Canada, Global Biogeochem. Cy., 21, GB4004, doi:10.1029/2006GB002866, 2007.
Reimer, P. J., Brown, T. A., and Reimer, R. W.: Discussion: reporting and calibration of post-bomb ^{14}C data, Radiocarbon, 46, 1299–1304, 2004.
Romanovsky, V. E., Smith, S. L., and Christiansen, H. H.: Permafrost thermal state in the polar Northern Hemisphere during the international polar year 2007–2009: a synthesis, Permafrost Periglac., 21, 106–116, doi:10.1002/ppp.689, 2010.
Schuur, E. A. G., McGuire, A. D., Schadel, C., Grosse, G., Harden, J. W., Hayes, D. J., Hugelius, G., Koven, C. D., Kuhry, P., Lawrence, D. M., Natali, S. M., Olefeldt, D., Romanovsky, V. E., Schaefer, K., Turetsky, M. R., Treat, C. C., and Vonk, J. E.: Climate change and the permafrost carbon feedback, Nature, 520, 171–179, doi:10.1038/nature14338, 2015.
Sepulveda-Jauregui, A., Walter Anthony, K. M., Martinez-Cruz, K., Greene, S., and Thalasso, F.: Methane and carbon dioxide emissions from 40 lakes along a north–south latitudinal transect in Alaska, Biogeosciences, 12, 3197–3223, doi:10.5194/bg-12-3197-2015, 2015.
Smith, S. and Burgess, M. M.: Ground Temperature Database for Northern Canada, Open File Report 3954, Geological Survey of Canada, Ottawa, 28 pp., 2000.
Southon, J. and Santos, G. M.: Life with MC-SNICS. Part II: Further ion source development at the Keck carbon cycle AMS facility, Nucl. Instrum. Meth. B, 259, 88–93, doi:10.1016/j.nimb.2007.01.147, 2007.
Stainton, M. P., Capel, M. J., and Armstrong, F. A. J.: The Chemical Analysis of Fresh Water, 2nd. edn., Serv., C. F. M., Misc. Spec. Publ., 25, 1977.
Stepanenko, V. M., Machul'skaya, E. E., Glagolev, M. V., and Lykossov, V. N.: Numerical modeling of methane emissions from lakes in the permafrost zone, Izv. Atmos. Ocean. Phy.+, 47, 252–264, doi:10.1134/s0001433811020113, 2011.
Stuiver, M. and Polach, H. A.: Discussion: reporting ^{14}C data, Radiocarbon, 19, 355–363, 1977.
Tarnocai, C., Canadell, J. G., Schuur, E. A. G., Kuhry, P., Mazhitova, G., and Zimov, S.: Soil organic carbon pools in the northern circumpolar permafrost region, Global Biogeochem. Cy., 23, GB2023, doi:10.1029/2008GB003327, 2009.
Tedford, E. W., MacIntyre, S., Miller, S. D., and Czikowsky, M. J.: Similarity scaling of turbulence in a temperate lake during fall cooling, J. Geophys. Res.-Oceans, 119, 4689–4713, doi:10.1002/2014JC010135, 2014.

BGD
12, 11661–11705, 2015

Tremblay, S., Bhiry, N., and Lavoie, M.: Long-term dynamics of a palsa in the sporadic permafrost zone of northwestern Quebec (Canada), Can. J. Earth Sci., 51, 500–509, doi:10.1139/cjes-2013-0123, 2014.
van Huissteden, J., Berrittella, C., Parmentier, F. J. W., Mi, Y., Maximov, T. C., and Dolman, A. J.: Methane emissions from permafrost thaw lakes limited by lake drainage, Nat. Clim. Chang., 1, 119–123, doi:10.1038/nclimate1101, 2011.
Vonk, J. E. and Gustafsson, O.: Permafrost-carbon complexities, Nat. Geosci., 6, 675–676, doi:10.1038/ngeo1937, 2013.
Vonk, J. E., Mann, P. J., Davydov, S., Davydova, A., Spencer, R. G. M., Schade, J., Sobczak, W. V., Zimov, N., Zimov, S., Bulygina, E., Eglinton, T. I., and Holmes, R. M.: High biolability of ancient permafrost carbon upon thaw, Geophys. Res. Lett., 40, 2689–2693, doi:10.1002/grl.50348, 2013.
Walter, K. M., Smith, L. C., and Chapin, F. S.: Methane bubbling from northern lakes: present and future contributions to the global methane budget, Philos. T. R. Soc. A, 365, 1657–1676, doi:10.1098/rsta.2007.2036, 2007.
Walter, K. M., Chanton, J. P., Chapin, F. S., Schuur, E. A. G., and Zimov, S. A.: Methane production and bubble emissions from arctic lakes: isotopic implications for source pathways and ages, J. Geophys. Res.-Biogeo., 113, G00A08, doi:10.1029/2007jg000569, 2008.
Walter Anthony, K. M. and Anthony, P.: Constraining spatial variability of methane ebullition seeps in thermokarst lakes using point process models, J. Geophys. Res.-Biogeo., 118, 1015–1034, doi:10.1002/jgrg.20087, 2013.
Walter Anthony, K. M., Vas, D. A., Brosius, L., Chapin, F. S., Zimov, S. A., and Zhuang, Q. L.: Estimating methane emissions from northern lakes using ice-bubble surveys, Limnol. Oceanogr.-Meth., 8, 592–609, doi:10.4319/lom.2010.8.0592, 2010.
Wanninkhof, R.: Relationship between wind-speed and gas-exchange over the ocean, J. Geophys. Res.-Oceans, 97, 7373–7382, doi:10.1029/92jc00188, 1992.
Whiticar, M. J.: Carbon and hydrogen isotope systematics of bacterial formation and oxidation of methane, Chem. Geol., 161, 291–314, doi:10.1016/S0009-2541(99)00092-3, 1999.
Whiticar, M. J., Faber, E., and Schoell, M.: Biogenic methane formation in marine and freshwater environments: CO_2 reduction vs. acetate fermentation – isotope evidence, Geochim. Cosmochim. Ac., 50, 693–709, doi:10.1016/0016-7037(86)90346-7, 1986.

BGD
12, 11661–11705, 2015

Wik, M., Crill, P. M., Bastviken, D., Danielsson, A., and Norback, E.: Bubbles trapped in arctic lake ice: potential implications for methane emissions, J. Geophys. Res.-Biogeo., 116, 10, doi:10.1029/2011jg001761, 2011.

Wik, M., Crill, P. M., Varner, R. K., and Bastviken, D.: Multiyear measurements of ebullitive methane flux from three subarctic lakes, J. Geophys. Res.-Biogeo., 118, 1307–1321, doi:10.1002/jgrg.20103, 2013.

Xu, X., Trumbore, S. E., Zheng, S., Southon, J. R., McDuffee, K. E., Luttgen, M., and Liu, J. C.: Modifying a sealed tube zinc reduction method for preparation of AMS graphite targets: reducing background and attaining high precision, Nucl. Instrum. Methods B, 259, 320–329, doi:10.1016/j.nimb.2007.01.175, 2007.

Zimov, S. A., Voropaev, Y. V., Semiletov, I. P., Davidov, S. P., Prosiannikov, S. F., Chapin, F. S., Chapin, M. C., Trumbore, S., and Tyler, S.: North Siberian lakes: a methane source fueled by Pleistocene carbon, Science, 277, 800–802, doi:10.1126/science.277.5327.800, 1997.

Zimov, S. A., Schuur, E. A. G., and Chapin, F. S.: Permafrost and the global carbon budget, Science, 312, 1612–1613, doi:10.1126/science.1128908, 2006.

Zona, D., Lipson, D. A., Paw, K. T., Oberbauer, S. F., Olivas, P., Gioli, B., and Oechel, W. C.: Increased CO_2 loss from vegetated drained lake tundra ecosystems due to flooding, Global Biogeochem. Cy., 26, GB2004, doi:10.1029/2011gb004037, 2012.

BGD
12, 11661–11705, 2015

Table 1. Limnological properties of ponds and lakes sampled in July 2013 and July 2014, including sampling depth, dissolved organic carbon (DOC), total phosphorus (TP), soluble reactive phosphorus (SRP), total nitrogen (TN), and selected major ions (NO_3, SO_4, Fe, Mn). POL = polygonal pond; IWT = ice wedge trough pond; LAK = lake.

Site	Type	Depth (m)	DOC ($mg\,L^{-1}$)	TP ($\mu g\,L^{-1}$)	SRP ($\mu g\,L^{-1}$)	TN ($mg\,L^{-1}$)	NO_3 ($mg\,L^{-1}$)	SO_4 ($mg\,L^{-1}$)	Fe ($mg\,L^{-1}$)	Mn ($mg\,L^{-1}$)
				2013						
BYL30	POL	surf	8.69	14.8	N/A	0.49	0.42	1.26	0.470	0.0158
BYL80	POL	surf	5.63	22.9	N/A	0.42	0.09	1.27	0.250	0.0045
Average POL (*n* = 9)			*6.67*	*17.6*		*0.47*	*0.17*	*1.34*	*0.282*	*0.0064*
BYL24	IWT	surf	6.56	16.1	N/A	0.29	0.37	4.32	0.270	0.0137
BYL27	IWT	surf	10.06	29.0	N/A	0.58	0.07	6.19	1.400	0.0184
Average IWT (*n* = 12)			*10.02*	*27.8*		*0.63*	*0.19*	*6.70*	*1.014*	*0.0240*
BYL66	LAK	surf	4.16	20.7	N/A	0.27	0.13	2.90	0.460	0.0038
BYL36*	LAK	surf	3.94	16.2	0.33	0.22	0.10	1.70	0.067	0.0069
				2014						
BYL30	POL	surf	12.20	8.5	1.31	1.32	0.25	2.60	0.648	0.0280
BYL80	POL	surf	10.60	22.7	1.75	1.25	< 0.2	1.60	0.266	0.0086
BYL24	IWT	surf	8.80	23.7	1.28	1.02	0.30	1.30	1.549	0.0380
		0.9	9.30	21.5	1.95	1.16	0.21	1.70	2.169	0.0026
BYL27	IWT	surf	12.10	27.4	1.56	1.22	0.29	2.70	0.487	0.0022
		1.3	14.30	54.8	1.41	1.70	0.25	2.40	2.979	0.1430
BYL66	LAK	surf	4.30	9.8	< 0.5	0.49	< 0.2	2.40	2.949	0.0849
		2.0	4.20	10.6	0.74	0.44	< 0.2	2.50	0.627	0.0198
		4.5	4.10	28.0	0.75	0.56	0.27	2.60	0.507	0.0013
BYL36	LAK	surf	4.30	6.7	1.13	0.45	0.27	2.20	0.023	0.0011
		2.0	4.20	-	0.91	0.46	< 0.2	2.20	0.027	0.0006
		10.0	4.20	41.2	1.29	0.57	< 0.2	2.30	0.039	0.0210

* 2011 data.

BGD
12, 11661–11705, 2015

Table 2. Greenhouse gas radiocarbon and stable isotope results for the six priority ponds and lakes sampled during two consecutive years (2013 and 2014). Active layer samples collected in 2013 near two trough ponds are also included. POL = polygonal pond; IWT = ice wedge trough pond; LAK = lake; UAL = upper active layer (0–5 cm); LAL = lower active layer (50–60 cm); Fm = fraction modern.

Year	Site	Type	Gaseous CO_2 ppmv	Gaseous CH_4 ppmv	Fm CO_2	Fm CH_4	$\Delta^{14}C$ CO_2 (‰)	$\Delta^{14}C$ CH_4 (‰)	^{14}C age CO_2 (BP)	^{14}C age CH_4 (BP)	$\delta^{13}C$ CO_2 vs. VPDB	$\delta^{13}C$ CH_4 vs. VPDB	δD CH_4 vs. VSMOW
2013	BYL30	POL	2580	324 066	1.022	1.060	14	52	> Modern	> Modern	−10.6	−63.3	−378
2013	BYL80	POL	29124	784 232	1.001	1.027	−7	20	0	> Modern	0.3	−67.6	−347
2013	BYL80	POL	735	234 455	0.987	1.006	−21	−1	105	> Modern	−13.7	−65.7	−356
2013	BYL24	IWT	5783	115 383	0.987	1.031	−20	23	105	> Modern	−21.8	−61.5	−398
2013	BYL27	IWT	1542	77 007	0.934	1.010	−73	2	550	> Modern	−17.4	−60.1	−399
2013	BYL66	LAK	5269	324 781	0.837	0.788	−169	−218	1425	1910	−8.4	−63.2	−392
2014	BYL30	POL	1607	18 406	1.021	1.073	13	64	Modern	> Modern	−18.1	−57.7	−352
2014	BYL30	POL	2857	15 724	N/A	N/A	N/A	N/A	N/A	N/A	−16.2	−52.1	−384
2014	BYL80	POL	< 50	174 762	1.010	1.067	3	58	Modern	Modern	N/A	−53.9	−346
2014	BYL80	POL	< 50	232 178	0.970	1.076	−38	68	245	> Modern	N/A	−56.5	−372
2014	BYL24	IWT	< 50	330 145	1.049	1.043	41	35	Modern	Modern	N/A	−63.0	−426
2014	BYL27	IWT	32383	291 005	0.996	1.000	−12	−8	35	5	−16.1	−59.3	−410
2014	BYL27	IWT	< 50	251 821	1.009	1.006	1	−2	Modern	Modern	N/A	−59.9	−448
2014	BYL66	LAK	1774	31 124	0.935	0.824	−72	−182	540	1555	−17.9	−59.9	−387
2014	BYL66	LAK	< 50	436 334	0.909	0.680	−98	−326	765	3105	N/A	−59.2	−344
2014	BYL66	LAK	< 50	330 116	0.939	0.655	−69	−350	510	3405	N/A	−57.4	−320
2014	BYL36	LAK	< 50	25 187	0.886	0.984	−121	−23	970	125	N/A	−63.1	−379
2014	BYL36	LAK	3845	1761	N/A	N/A	N/A	N/A	N/A	N/A	−17.5	−65.5	−345
2013	BYL27 (UAL)	IWT	N/A	N/A	1.062		62		> Modern		−28.9		N/A
2013	BYL27 (LAL)	IWT	N/A	N/A	0.730		−270		2535		−26.3		N/A
2013	BYL28 (UAL)	IWT	N/A	N/A	1.000		−1		5		N/A		N/A
2013	BYL28 (LAL)	IWT	N/A	N/A	0.759		−241		2210		N/A		N/A

BGD
12, 11661–11705, 2015

Table 3. Diffusive and ebullition fluxes of CO_2 and CH_4 for the six priority ponds and lakes sampled during two consecutive years (2013 and 2014). POL = polygonal pond; IWT = ice wedge trough pond; LAK = lake; Min = minimum; Med = median; Max = maximum.

			Diffusive fluxes ($mmol\,m^{-2}\,d^{-1}$)						Ebullition fluxes ($mmol\,m^{-2}\,d^{-1}$)						
			CO_2			CH_4				CO_2			CH_4		
Site	Type	N	Min	Med	Max	Min	Med	Max	N	Min	Med	Max	Min	Med	Max
BYL30	POL	12	−8.11	−1.04	5.73	0.19	1.07	1.46	12	0.00	0.01	0.26	0.01	0.89	26.57
BYL80	POL	32	−11.78	−3.14	45.44	0.03	0.53	1.14	9	0.00	0.00	16.32	0.11	0.99	534.54
All	*POL*	*44*	*-11.78*	*-2.98*	*45.44*	*0.03*	*0.53*	*1.46*	*21*	*0.00*	*0.01*	*16.32*	*0.01*	*0.99*	*534.54*
BYL24	IWT	18	−5.44	13.27	26.30	0.05	0.17	1.51	8	0.00	0.00	0.02	0.01	0.06	0.29
BYL27	IWT	26	15.96	25.86	65.50	0.34	1.03	5.82	11	0.00	0.00	5.18	0.00	4.55	32.93
All	*IWT*	*44*	*-5.44*	*21.76*	*65.50*	*0.05*	*0.99*	*5.82*	*19*	*0.00*	*0.00*	*5.18*	*0.00*	*0.06*	*32.93*
BYL66	LAK	12	−7.05	1.62	5.13	0.06	0.09	0.27	11	0.00	0.00	0.00	0.00	0.15	5.08
BYL36	LAK	6	−0.75	1.20	1.37	0.06	0.08	1.13	2	0.00	0.00	0.00	0.00	0.02	0.03
All	*LAK*	*18*	*-7.05*	*1.30*	*5.13*	*0.06*	*0.09*	*1.13*	*13*	*0.00*	*0.00*	*0.00*	*0.00*	*0.15*	*5.08*
All water bodies		***106***	***−11.78***	***1.74***	***65.50***	***0.03***	***0.54***	***5.82***	***53***	***0.00***	***0.00***	***16.32***	***0.00***	***0.18***	***534.54***

BGD
12, 11661–11705, 2015

Table 4. Greenhouse gas fluxes of CO_2 and CH_4 from high-latitude sites across the circum-Arctic. D = diffusion; E = ebullition.

Reference	Region	Type	Mode	CO_2 mg C m^{-2} d^{-1} Min	CO_2 mg C m^{-2} d^{-1} Max	CH_4 mg C m^{-2} d^{-1} Min	CH_4 mg C m^{-2} d^{-1} Max	Notes
Bouchard et al. (2015)	NE Canada	Polygon ponds	D + E	−141.4	741.1	0.5	6432.0	July measurements
		Troughs	D + E	−65.3	848.1	2.6	465.1	
		Lakes	D + E	−84.6	61.6	0.7	74.5	
Laurion et al. (2010)	NE Canada	Subarctic ponds	D	27.6	746.4	0.4	5.4	July measurements
		Arctic ponds	D	−246.0	1372.8	0.4	67.4	
		Arctic lakes	D	−63.6	70.8	0.1	0.4	
Buell (2014)	NW Canada	Ponds	D + E	−3.5	120.0			Headspace, chamber and flux tower methods
Kling et al. (1992)	Alaska	Lakes and rivers	D	−66.0	717.6	1.0	12.2	25 lakes + 4 rivers
Walter Anthony and Anthony (2013)	Alaska	Thermokarst lakes	E			0.6	155.7	Strongest emissions = submerged polygons (lake shore)
Sepulveda-Jauregui et al. (2014)	Alaska	Lakes	D + E	51.9	2276.9	3.0	455.4	Annual fluxes (ice-free period = 180 days)
Walter Anthony et al. (2010)	Alaska, Siberia	Thermokarst lakes	E			0.0	18716.8	Background + seep ebullition
Abnizova et al., 2012	Siberia	Whole landscape	D + E	200.0	1100.0			September measurements, flux tower
Blodau et al. (2008)	Siberia	Ponds	D	Average = 20.5		82.3	127.2	
Kankaala et al. (2013)	Finland	Lakes	D	140.0	1586.7	0.2	26.7	Annual fluxes (ice-free period = 180 days)
Huttunen et al. (2003)	Finland	Lakes and reservoirs	D + E	−21.6	876.0	0.8	99.6	CO_2 = diffusion only
Bastviken et al. (2004)	Sweden	Lakes	D			0.6	11.0	Annual fluxes (ice-free period = 180 days)

BGD
12, 11661–11705, 2015

Table B1. Temperature and total precipitation data for the six months preceding the sampling period in July 2013 and 2014. The climate normal (1981–2010) is also indicated (Environment Canada, 2015).

	Temperature (°C)			Precipitation (mm)		
Month	2013	2014	Normal	2013	2014	Normal
Jan	−28.7	−30.8	−33.4	13.4	1.5	4.8
Feb	−30.5	−32.7	−33.7	0.0	0.4	3.8
Mar	−22.2	−29.8	−30.0	22.0	0.0	6.6
Apr	−19.5	−19.8	−21.8	14.2	1.6	10.5
May	−12.4	−7.2	−9.3	0.0	17.6	9.4
Jun	3.4	2.5	2.4	20.7	5.9	15.6
Total (Jan–Jun)	−18.3	−19.6	−21.0	70.3	27.0	50.7

BGD
12, 11661–11705, 2015

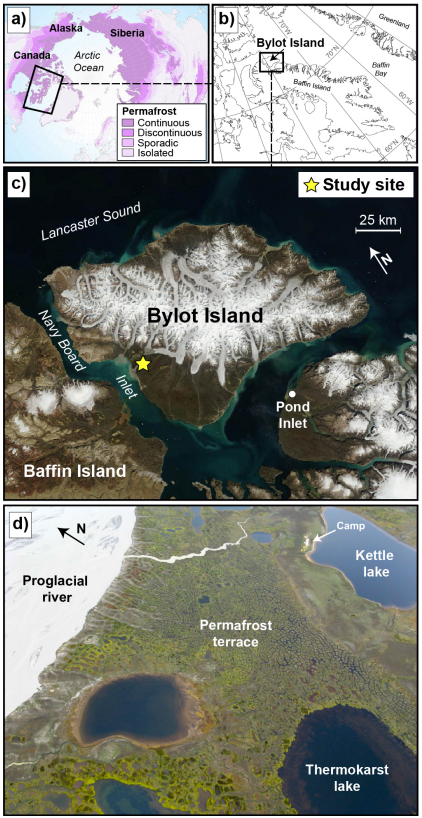

Figure 1. Location of the study site in the continuous permafrost zone of the eastern Canadian Arctic **(a)**, north of Baffin Island **(b)**, within one of the several glacier valleys of Bylot Island, Nunavut **(c)**. The studied valley contains numerous aquatic systems of different sizes **(d)**. Source of the permafrost map **(a)**: Brown et al. (1998). Satellite photo **(c)**: Terra-MODIS, 22 July 2012.

BGD
12, 11661–11705, 2015

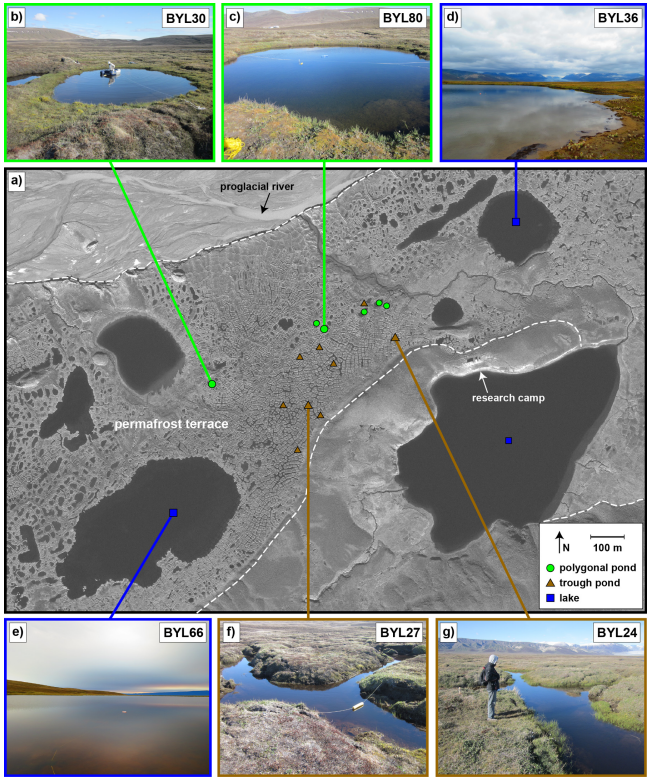

Figure 2. Location of the sampled water bodies **(a)**, including polygonal ponds **(b, c)**, kettle and thermokarst lakes (**d** and **e**, respectively) and trough ponds **(f, g)**. Ponds and lakes are located within the limits of a peaty loess permafrost terrace, outlined with the dashed white line. Satellite photo **(a)**: GeoEye-1, 18 July 2010.

BGD
12, 11661–11705, 2015

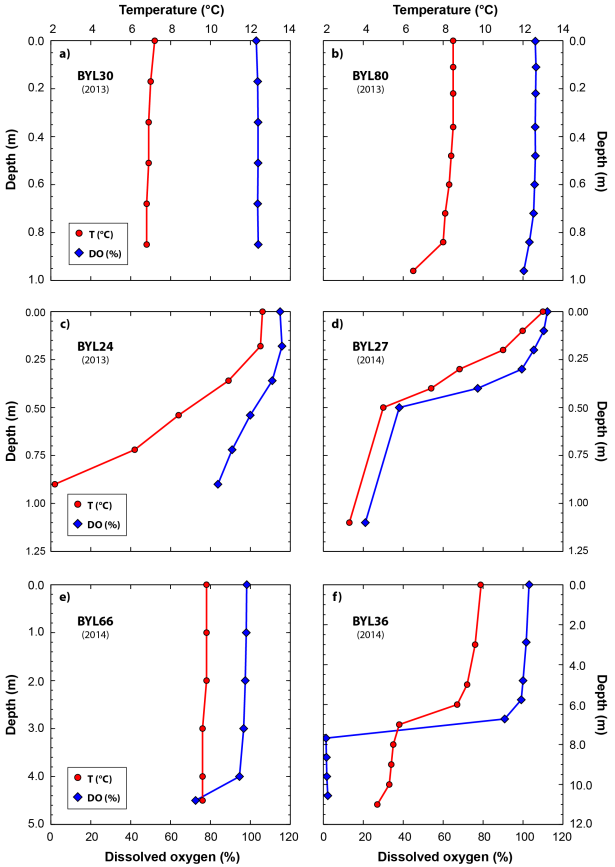

Figure 3. Temperature (°C; upper *x* axes) and dissolved oxygen (%; lower *x* axes) profiles for polygonal ponds BYL30 **(a)** and BYL80 **(b)**, trough ponds BYL24 **(c)** and BYL27 **(d)**, and lakes BYL66 **(e)** and BYL36 **(f)**. Some profiles **(a–c)** were taken in July 2013, whereas the others **(d–f)** were taken in July 2014. Note the different vertical scales (depth).

BGD
12, 11661–11705, 2015

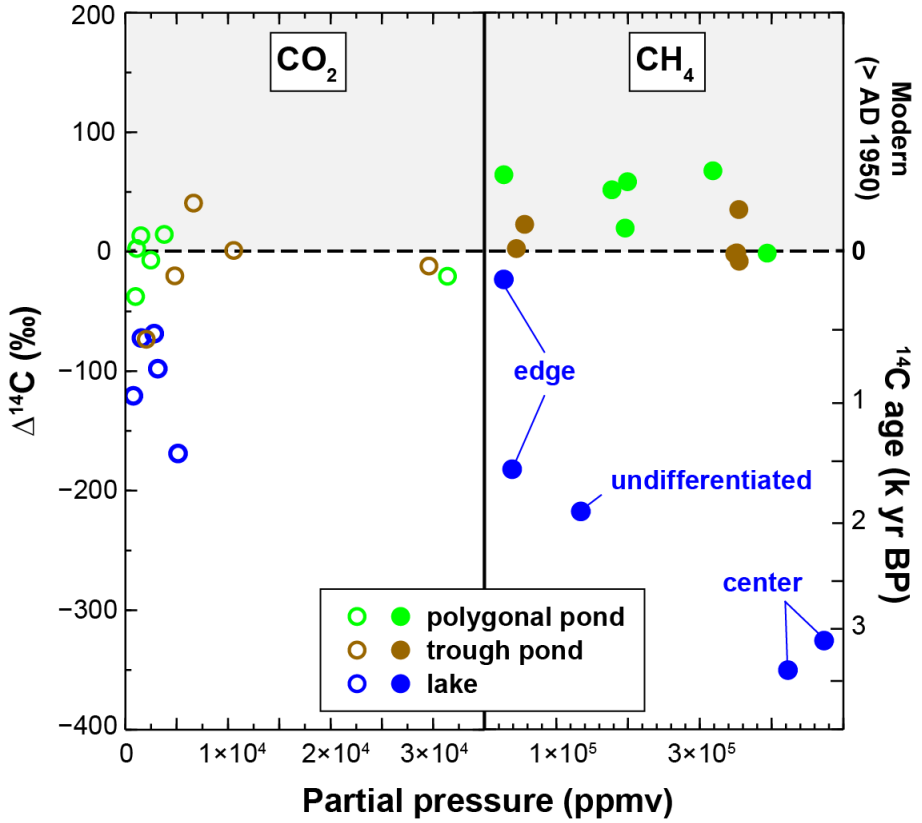

Figure 4. Concentration and age of ebullition GHG collected from ponds and lakes on Bylot Island, Nunavut. Gas concentration (*x* axis) is expressed as partial pressure (in ppmv, parts per million volumetric) of CO_2 (open circles) and CH_4 (full circles). Radiocarbon age is expressed as the normalized radiocarbon activity ($\Delta^{14}C$, in ‰ ; left *y* axis) corrected for isotopic fractionation and decay that took place between sampling and measurement dates, and in thousands of years before present (k yr BP; right *y* axis).

BGD
12, 11661–11705, 2015

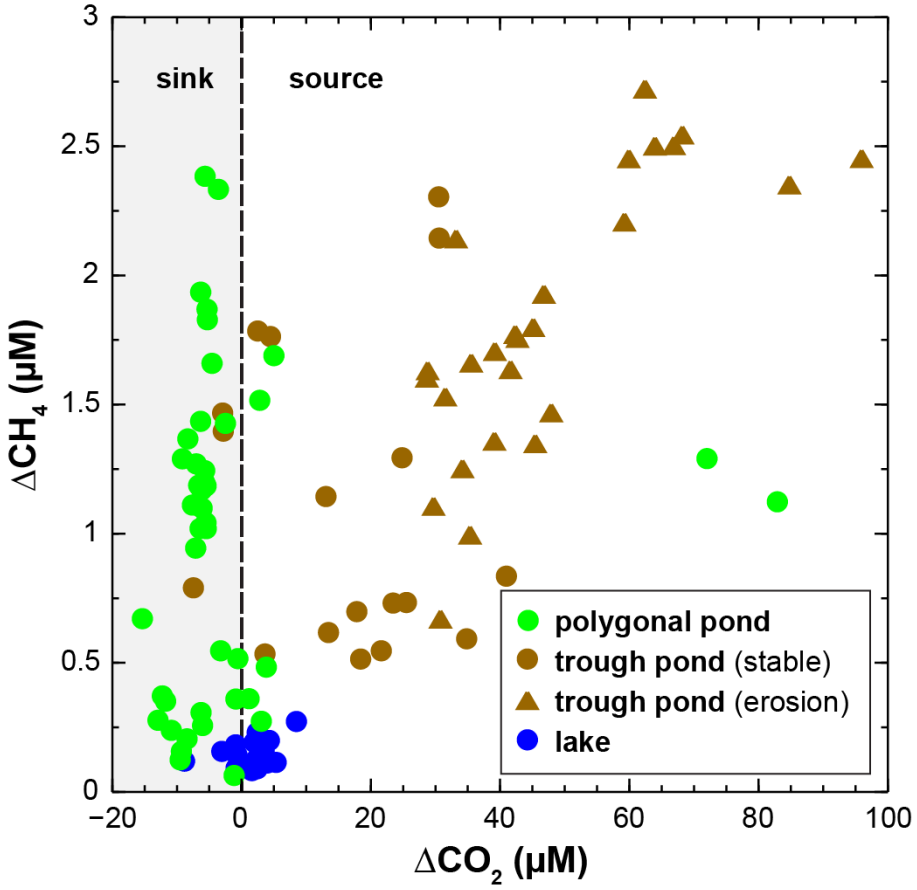

Figure 5. Saturation levels of dissolved GHG in pond and lake water. Values are expressed as the departure from saturation (in µM) for CO_2 (x axis) and CH_4 (y axis). Values < 0 indicate a sink, whereas values > 0 indicate a source.

BGD
12, 11661–11705, 2015

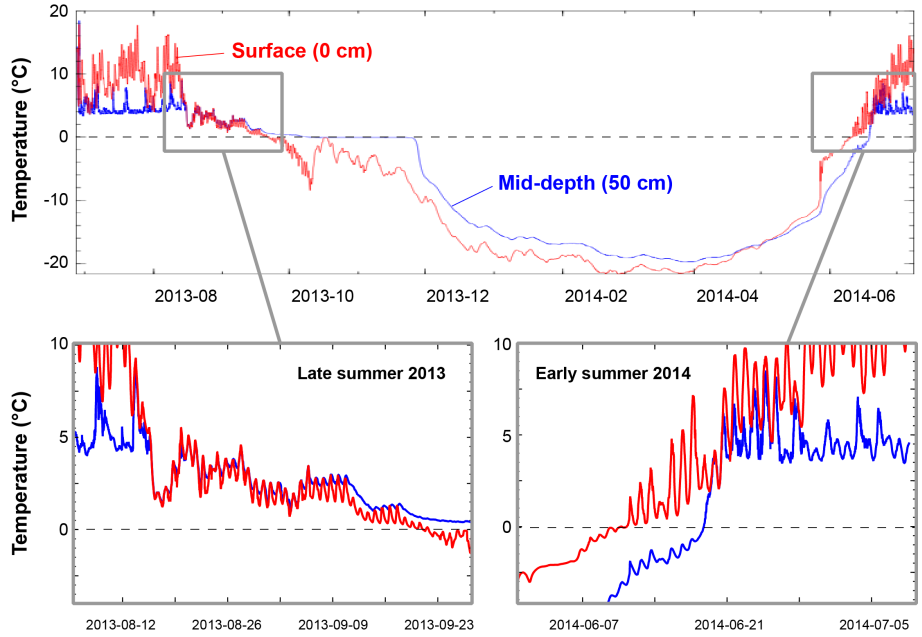

Figure 6. Water temperature at two depths (surface = 0 cm; mid-depth = 50 cm) in trough pond BYL27 over one year (27 June 2013 to 08 July 2014), showing extended stratification and rare mixing events (lower panels) during the summer.

BGD
12, 11661–11705, 2015

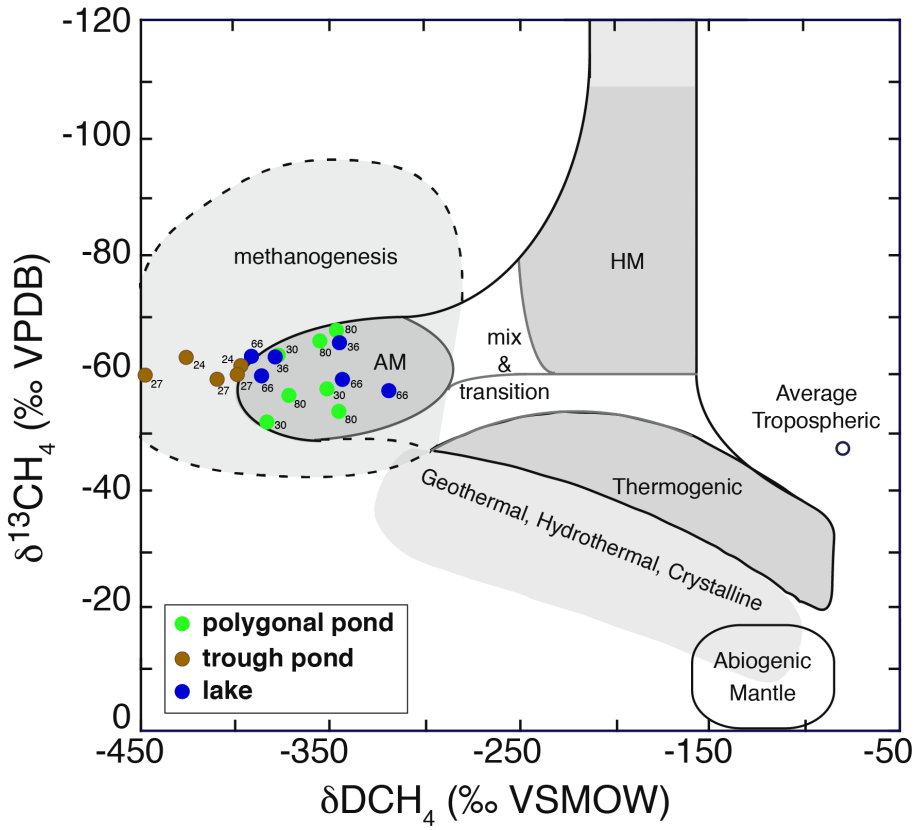

Figure 7. Carbon (δ^{13}) and hydrogen (δD) isotope composition of the methane emitted through ebullition by the sampled ponds and lakes, after Whiticar et al. (1986). AM = acetoclastic methanogenesis; HM = hydrogenotrophic methanogenesis.

BGD
12, 11661–11705, 2015

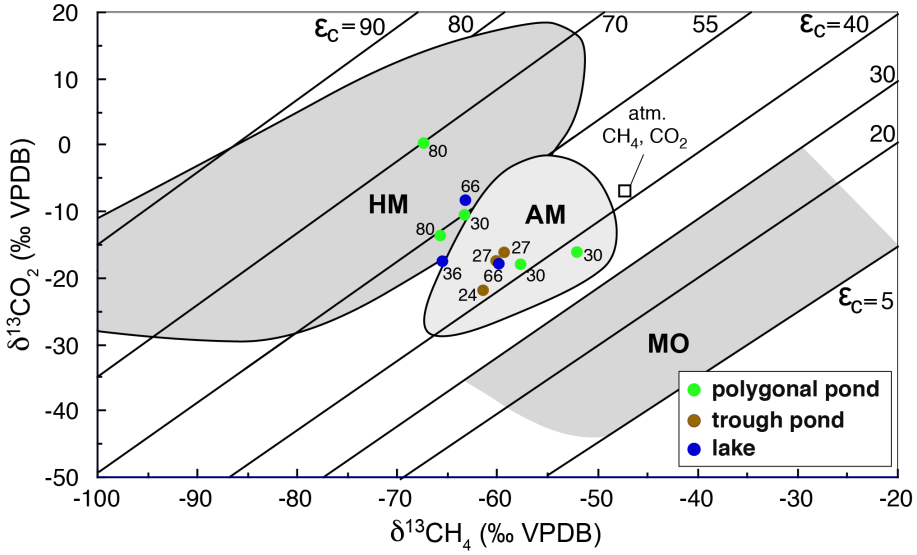

Figure 8. Carbon isotope composition ($\delta^{13}C$) of CH_4 (x axis) and CO_2 (y axis) emitted by the sampled ponds and lakes. HM = hydrogenotrophic methanogenesis; AM = acetoclastic methanogenesis; MO = methane oxidation.

BGD
12, 11661–11705, 2015

Figure A1. Picture of the homemade funnels deployed in ponds and lakes (photo taken in July 2014 just after their removal).

BGD
12, 11661–11705, 2015

Figure C1. Picture of eroding shores (slumping peat) along trough pond BYL27 (photo taken in July 2014). The sampling funnel syringe can be seen just above the water surface.

BGD
12, 11661–11705, 2015

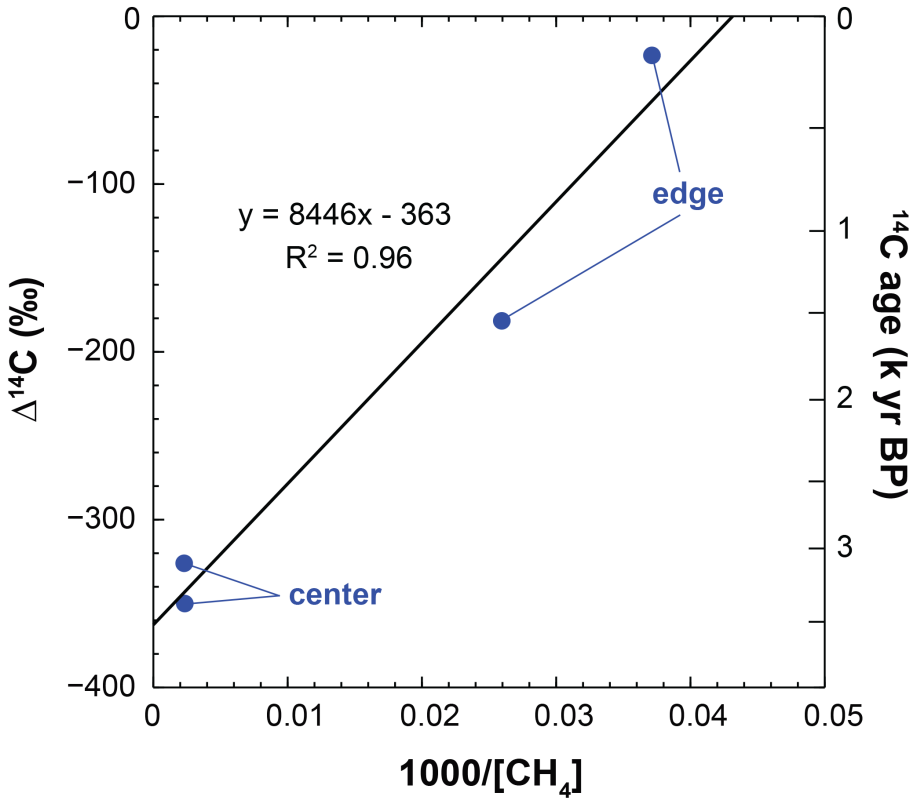

Figure D1. Keeling plot of lake ebullition CH_4 sampled in 2014, showing a mixing of millennium-old and highly concentrated with near-modern and less concentrated gas. Concentration (x axis) is expressed as 1000/partial pressure (in ppmv, parts per million volumetric), whereas radiocarbon age is expressed as the normalized radiocarbon activity ($\Delta^{14}C$, in ‰; left y axis) and in thousands of years before present (kyr BP; right y axis).

BGD
12, 11661–11705, 2015